

Investigation on growth, optical and thermal properties of stilbazolium derivative crystal: 4-N,N-dimethylamino-4'-N'-methylstilbazolium 2,4-dimethylbenzenesulfonate

I. MD. ZAHID¹, S. KALAIYARASI¹, M. KRISHNA KUMAR², T. GANESH¹, V. JAISANKAR³,
R. MOHAN KUMAR^{1,*}

¹Department of Physics, Presidency College, Chennai, 600 005, India

²Department of Physics, Kalasalingam University, Krishnankoil, 626 126, India

³Department of Chemistry, Presidency College, Chennai, 600 005, India

Metathesis ionic exchange reaction process was used to synthesize a novel nonlinear optical material: 4-N,N-dimethylamino-4'-N'-methylstilbazolium 2,4-dimethylbenzenesulfonate (DSDMS). The growth of DSDMS single crystals was carried out by adopting the solution growth technique. The crystal perfection and lattice parameters were elucidated from single XRD and powder XRD, respectively and its morphology was interpreted by WinXMorph program. FT-IR and Raman spectral analyses confirmed the existence of functional groups and their corresponding vibrational modes. UV-Vis spectral studies revealed the optical transmission region. Mechanical stability of the crystal was determined from Vickers microhardness number H_v , Meyer's index n and elastic stiffness constant C_{11} . Dielectric and thermal behavior of the grown crystal were elucidated by using impedance analyser and thermogravimetric analysis.

Keywords: ionic crystals; DSDMS; solution growth technique; nonlinear optical material

© Wrocław University of Technology.

1. Introduction

The organic crystals are being recently a source of interest as terahertz (THz) emitters as they have been reported to generate stronger THz signals than commonly used semiconductors or inorganic emitters [1–4]. Much effort has been made to develop new materials with high second-order nonlinearities which are expected to support applications in the areas such as electro-optic switching for telecommunications [5], optical information processing [6], optical data storage [7, 8] and the generation of terahertz radiation [9]. Among the various classes of materials investigated worldwide, ionic organic NLO crystal 4-N,N-dimethylamino-4'-N'-methylstilbazolium tosylate (DAST)

derivatives are of special interest due to their advantageous mechanical, chemical and thermal properties [10]. In addition, the growth of highly nonlinear optical quality bulk crystals or thin films of DAST still remains a big challenge [11–13], therefore, novel materials with high nonlinear properties similar to those of DAST, but with superior growth possibilities are greatly desired. Minor modification of the counter-anion in the DAST structure, can produce novel stilbazolium derivatives with favourable non-centrosymmetric packing. Its characteristics may be superior to the parent ones due to the substitution of p-conjugated groups. 4-N,N-dimethylamino-4'-N'-methylstilbazolium 2,4-dimethylbenzenesulfonate (DSDMS) draw attention as one of the most useful nonlinear optical materials which has a large nonlinear coefficient. The second harmonic generation (SHG) efficiency of DSDMS is about 0.7 times

*E-mail: mohan66@hotmail.com

of DAST [14]. The very highly nonlinear is the key parameter of DSDMS for electro-optical and THz generation measurements. DSDMS render itself as a good competitor crystal when compared with other existing nonlinear crystals. Its physical and chemical properties, including structural, morphological, optical, hardness, electrical and thermal ones have been studied in detail and reported for NLO applications.

2. Experimental

2.1. Synthesis, solubility and crystal growth

4-N,N-dimethylamino-4'-N'-methylstilbazolium 2,4-dimethylbenzenesulfonate (DSDMS) salt was synthesised in a two-step process (Fig. 1). The condensation reaction between 1,4-dimethylpyridinium iodide and N,N-dimethylaminobenzaldehyde in the presence of weak amine of piperidine was carried out to prepare DMSI salt [15, 16]. The equimolar ratio was used for the metathesis reaction between DMSI (2.73 mmol.%) and sodium 2,4-dimethylbenzenesulfonate (2.73 mmol.%) which were dissolved in aqueous solution separately and heated up to 70 °C. These two hot solutions were mixed together at the same temperature and stirred well for about half an hour. This temperature is preferable for the formation of DSDMS salt by ionic exchange. Then, the solution was allowed to cool up to room temperature for a day. Due to the anion exchange between 4-N,N-dimethylamino-4'-N'-methylstilbazolium iodide (DMSI) and sodium 2,4-dimethylbenzenesulfonate at 70 °C, DSDMS precipitate has been obtained. The aqueous sodium iodide was separated from the DSDMS by gravity filtration method. The purity of DSDMS salt was improved by repeated recrystallization process with methanol solvent and the purified salt was used for qualitative and quantitative studies.

The solubility of the DSDMS salt was studied by using different solvents in pure or mixed forms to understand the growth parameters of DSDMS. Initially, various combinations of solvents were taken on a trial and

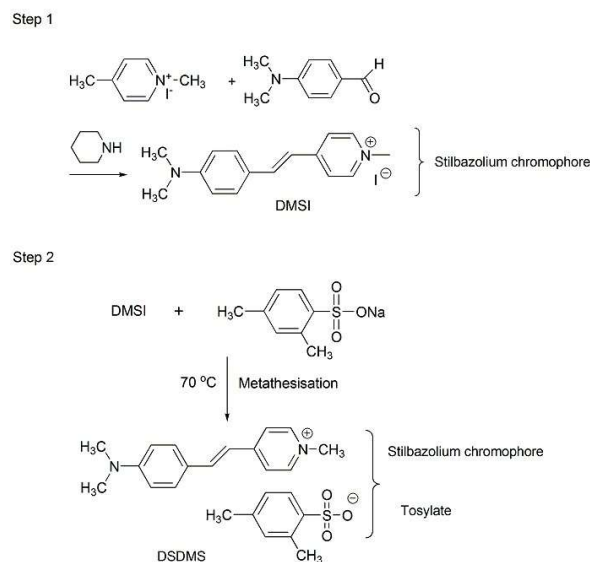


Fig. 1. Synthesis scheme of DSDMS.

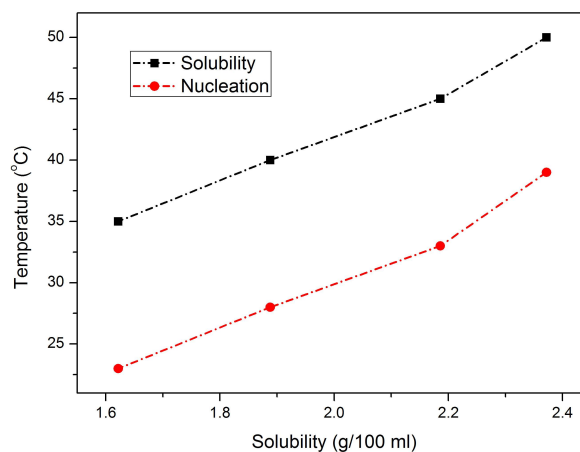


Fig. 2. Solubility and nucleation curves of DSDMS.

error basis, which were methanol, acetonitrile, methanol-water, acetonitrile-water and methanol-acetonitrile. However, DSDMS crystal formation was observed only in the methanol solvent system, and for other systems, the crystallization had rarely appeared. The solubility and nucleation curves of DSDMS are depicted in Fig. 2. The positive solubility coefficient is convenient to grow bulk crystals by both slow evaporation and cooling methods.

According to the solubility data, a measured quantity of DSDMS salt was dissolved in methanol and the saturated solution was prepared. The clear

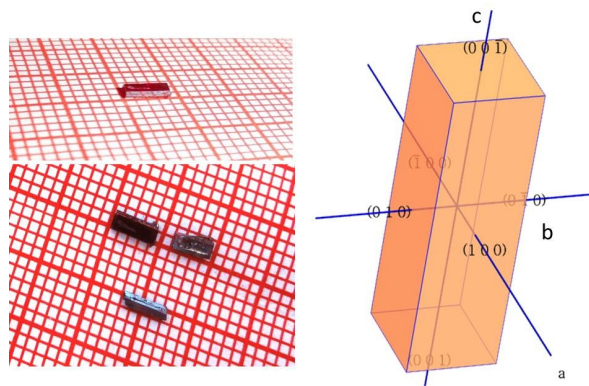


Fig. 3. Photograph of as-grown DSDMS single crystal and its prominent planes drawn with WinX-Morph program.

saturated solution was transferred to the crystal growth container. The saturated growth solution was allowed to evaporate slowly by keeping it in a constant temperature bath at 38 °C. Due to the solvent evaporation, the solution reached the supersaturated state and it spontaneously yielded (60 %) crystals with dimension up to $4 \times 2 \times 2 \text{ mm}^3$ in the period of 4–5 weeks (Fig. 3). The grown crystals were kept in safe environment and used for various characterizations to study its physical and chemical properties.

3. Results and discussion

3.1. Crystal structure and morphology

The single crystal X-ray diffraction data was recorded by using Bruker Kappa APEX II single crystal X-ray diffractometer. It indicates that the grown crystal belongs to triclinic crystal system with non-centrosymmetric P1 space group. The estimated cell dimensions are $a = 7.627 \text{ \AA}$, $b = 8.134 \text{ \AA}$, $c = 9.82 \text{ \AA}$, $\alpha = 72.14^\circ$, $\beta = 70.46^\circ$, $\gamma = 80.23^\circ$ and $V = 545.4 \text{ \AA}^3$ and it is in a good agreement with the reported data [14]. The crystal morphology was drawn by using WinXMorph program (Fig. 3). It indicates that the prominent growth direction is along c-axis which determines the length of the grown crystal. From the morphology of DSDMS, it is observed that the planes (1 0 0), (0 1 0) and (0 0 1) are perpendicular to each other. The DSDMS crystal was grinded to

uniform fine powder and subjected to powder X-ray diffraction study to reveal crystalline perfection of the compound. The peaks were indexed using PowderX program (Fig. 4) which shows the predominant planes of DSDMS crystal.

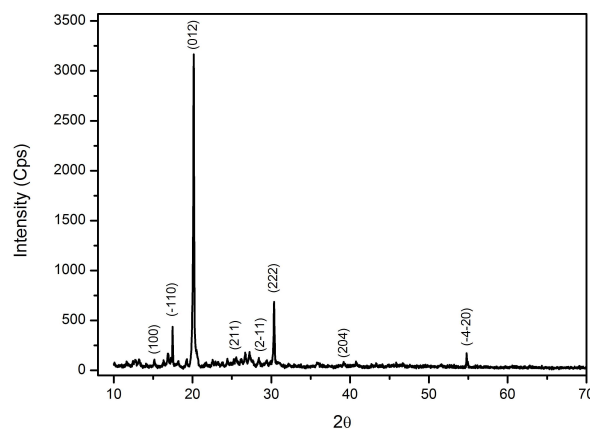


Fig. 4. Powder XRD pattern of DSDMS.

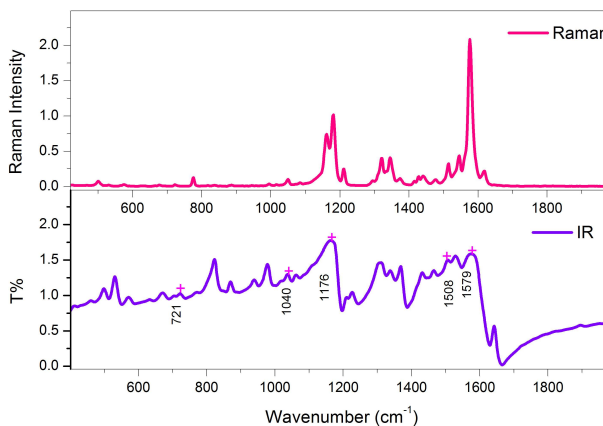


Fig. 5. Infrared and FT-Raman spectra of DSDMS.

3.2. IR and Raman spectral studies

4-N,N-dimethylamino-4'-N'-methylstilbazolium 2,4-dimethylbenzenesulfonate (DSDMS) crystal was powdered and FT-IR and FT-Raman spectra were recorded to identify the presence of functional groups. Fig. 5 shows the recorded infrared spectrum (400 cm^{-1} to 4000 cm^{-1}) and Raman spectrum (4000 cm^{-1} to 500 cm^{-1}) by using BRUKER IFS66VFT-IR and BRUKER RFS27 spectrometers, respectively.

IR spectrum shows the prominent bands of $\nu(\text{C}=\text{C})$ and $\nu(\text{C}-\text{C})$ of aromatic ring at 1579 cm^{-1} and 721 cm^{-1} , respectively. Aromatic ring chain vibrations observed at 1576 cm^{-1} are due to C-C vibration in Raman spectrum. The vibrational bands of IR spectrum at 1040 cm^{-1} , 1176 cm^{-1} and 1164 cm^{-1} are assigned to $\nu(\text{C}-\text{S})$, $\nu(\text{SO}_3)^-$ (asymmetric stretching) and $\nu(\text{SO}_3)^-$ (symmetric stretching). C=C stretching mode of unconjugated alkene gives absorption at 1600 cm^{-1} while the C-H stretching and bending vibrations of methyl group occur at 2850 cm^{-1} and 1360 cm^{-1} in the IR spectrum. In the Raman spectrum, a strong band observed at 775 cm^{-1} is due to C-S vibration. Also the vibrations of $\nu(\text{S}-\text{O})$ and $\nu(\text{C}-\text{N})$ stretchings appear at 679 cm^{-1} and 1508 cm^{-1} in the IR. Similarly, in Raman spectra, the weak band observed at 1049 cm^{-1} is due to S=O stretching vibration, and C-N stretching vibration is observed at 1210 cm^{-1} . The presence of CH_3 functional group and its vibrational modes was confirmed by the Raman spectrum. The out-of-plane bending of CH_3 functional group is observed at 1180 cm^{-1} . The weak symmetric stretching vibrational bands of CH_3 functional group are observed at 1345 cm^{-1} and 1373 cm^{-1} . The asymmetric in-plane stretching is observed as weak bands of CH_3 functional group at 1427 cm^{-1} and 1440 cm^{-1} . The aromatic or hetero ring mode is observed at 1544 cm^{-1} . The band noted at 1320 cm^{-1} evidences the C- CH_3 stretching vibration. The out-of-plane bending mode observed at 500 cm^{-1} is due to C- CH_3 vibration. From the IR and Raman spectra, all the prominent functional groups present in the DSDMS compound have been observed and presented in Table 1.

3.3. Optical studies

T90+UV-Vis Spectrophotometer was used to record the absorbance spectrum by dissolving the powdered sample in methanol (Fig. 6). It provides valuable information about the band gap, cut-off wavelength and transmission region of the grown DSDMS crystal. In addition, the structure of the

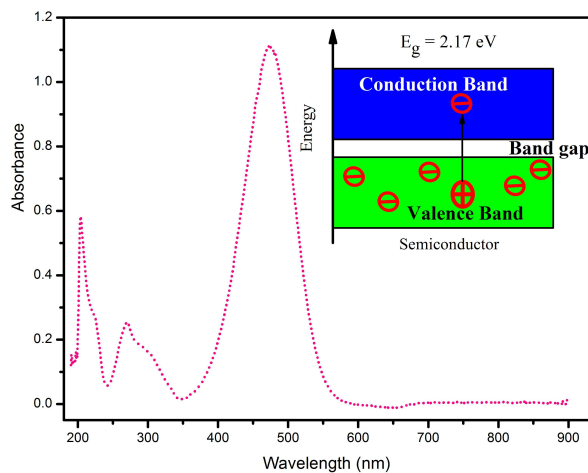


Fig. 6. UV-Vis absorption spectrum of DSDMS.

molecule has evolved, because the absorption of ultraviolet and visible light involve $\sigma - \sigma^*$ and $\pi - \pi^*$ orbital electronic transitions [17]. The recorded wavelength range is 190 nm to 900 nm. Any absorption of energy in the spectra indicates that ultraviolet and visible light involves the excitation of electrons from the ground state to excited energy states [18]. Fig. 6 illustrates that the DSDMS is transparent from 572 nm to 900 nm. Below the wavelength of 572 nm, the crystal is found to be opaque. It is evident that the DSDMS crystal has optical cut-off at 572 nm. Band gap energy (E_g) illustrates the conduction behavior and also its usefulness in optoelectronic devices. E_g value of the material is very closely related to the material's atomic and electronic band structures and is calculated using the relation [19]:

$$E_g = hc/\lambda \quad (1)$$

where h is Planck's constant, c is the velocity of light and λ is the cut-off wavelength for DSDMS (572 nm). The forbidden energy band gap (E_g) of the DSDMS crystal was found to be 2.17 eV. Since the electronic transition from the valence to conduction band span a fairly large range of energies, semiconductors act as a sort of a long pass filter (only reflecting light with energy less than the band gap). Also the band gap estimation (2.17 eV) confirms the semi-conducting behavior of DSDMS.

Table 1. Infrared and Raman band positions and their assignments of DSDMS.

$\nu_{\text{IR}} [\text{cm}^{-1}]$	$\nu_{\text{Raman}} [\text{cm}^{-1}]$	Assignments
	500	C-CH ₃ out-of-plane bending mode
679		S-O stretching
721		C-C aromatic ring
	775	C-S strong band
1040, 1176		C-S asymmetric stretching
	1049	S=O weak band
1164		SO ₃ symmetric stretching
	1180	CH ₃ out-of-plane bending
	1210	C-N stretching vibration
	1320	C-CH ₃ stretching vibration
	1345, 1373	CH ₃ weak band (symmetric stretching vibration)
	1400, 1650	C-C stretching modes
	1427, 1440	CH ₃ weak band (asymmetric in plane)
1360, 2850		C-H stretching and bending vibration of methyl group
1508		C-N stretching
	1544	Aromatic / hetero-strong
	1576	C-C aromatic ring chain vibration
1579		C=C aromatic ring
1600		C=C stretching mode unconjugated alkene

To evaluate the second harmonic generation (SHG) efficiency, the radiation with pulse energy of 1.2 mJ/pulse and wavelength $\lambda = 1064$ nm from an optical parametrical amplifier pumped by Nd:YAG laser has been used. After grinding, the microcrystalline powdered DSDMS sample of almost uniform size (~ 120 μm) has been filled in a capillary tube and exposed to laser irradiation. The incident beam generated the SHG signal from the DSDMS crystal (182 mV) which was about 1.52 times of KDP crystal (120 mV) and confirmed its suitability for the nonlinear optical applications.

3.4. Microhardness study

The structure and nature of bonding in crystalline solids have an influence on their mechanical hardness. Hardness of a material is influenced by various parameters such as lattice energy, Debye temperature, interplanar spacing and packing factor. The smooth and flat surface of (1 0 0) crystal plane was subjected to indentation test using Leitz-Wetzlar hardness tester fitted with a diamond

indenter and the measurements were made at room temperature. The load (P) of different magnitudes 25, 50, 75 and 100 g were applied. The Vicker's microhardness number (H_v) was calculated using the relation:

$$H_v = 1.8544P/d^2 \text{ kg/mm}^2 \quad (2)$$

where P is the applied load in g, d is the diagonal length of the indentation impression in mm and H_v is the hardness number in kg/mm^2 . The plot of Vicker's hardness number (H_v) against various loads is shown in Fig. 7. The Meyer's index number was calculated from the Meyer's law, which relates the load and indentation size:

$$P = k_1 d^n \quad (3)$$

where k_1 is the standard hardness constant and n is the work-hardening coefficient. A plot of log P versus log d was drawn (Fig. 7) and the value of n found from the slope of the graph was 2.45. According to Onitsch [20] and Hanneman [21], n should lie between 1 and 1.6 for comparatively

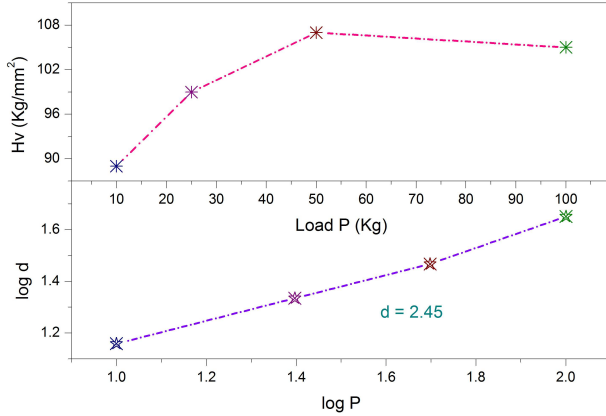


Fig. 7. Plots of hardness number (H_v) and Meyer index (d) versus load P of DSDMS.

hard materials, whereas it is above 1.6 for the softer ones. Thus, the grown DSDMS crystal belongs to the category of soft materials.

Hays and Kendall's [22] theory of resistance pressure was used to find the relationship between indentation test load (P) and indentation size (d) of DSDMS:

$$P - W = k_2 d^2 \quad (4)$$

where W is the resultant Newtonian pressure that represents the minimum load (P) which causes an indentation and k_2 is another constant. Using equation 3 and equation 4, the Newtonian resultant pressure (W) was calculated:

$$W = k_1 d^n - k_2 d^2 \quad (5)$$

The elastic-stiffness constant (C_{11}) was calculated using Wooster's empirical formula [23]:

$$C_{11} = (H_v)^{7/4} \quad (6)$$

This gives information about the bonding stiffness with neighboring atoms in DSDMS crystal. From the hardness value, the yield strength (σ_v) of DSDMS was calculated using the relation [24]:

$$\sigma_v = \frac{H_v}{2.9} \left[1 - (n-2) \left[\frac{12.5(n-2)}{1-(n-2)} \right] \right] \quad (7)$$

The calculated hardness value (H_v), Meyer's index (n), elastic stiffness constant (C_{11}) and yield strength (σ_v) are given in Table 2.

Table 2. Hardness parameters of DSDMS by using Vicker's hardness test.

Load [g]	H_v [$\text{kg}\cdot\text{mm}^{-2}$]	Meyers index [n]	C_{11} [GPa]	σ_v [GPa]
10	89.29	2.45	1.13	0.209
25	99.36	2.45	2.39	0.313
50	107.15	2.45	4.05	0.395
100	92.50	2.45	1.44	0.309

3.5. Dielectric and thermal analyses

Dielectric response in crystals reveals information about the electric field distribution and charge transport mechanism. The dielectric studies of DSDMS crystal was carried out using a HIOKI 3532 LCR HITESTER instrument in the frequency range 50 Hz to 5 MHz. To guarantee the precision of data, the sample of a thickness about 1 mm was used. Then, the opposite faces of the sample were covered by silver paste to make a parallel plate capacitor, and mounted between two electrodes. The capacitance of the parallel plate capacitor with the sample as dielectric medium was measured at 40 and 60 °C. The dielectric constant (ϵ') was calculated using the relation:

$$\epsilon' = Cd/\epsilon_0 A \quad (8)$$

where C is the capacitance, d is the thickness of the crystal, ϵ_0 is the permittivity of free space, and A is the area of the crystal. The dielectric loss (ϵ'') was calculated using the relation:

$$\epsilon'' = \epsilon' D \quad (9)$$

where D is the dissipation factor. Fig. 8a and Fig. 8b show the variation of the dielectric constant and dielectric loss for different frequencies keeping temperatures at 40 °C and 60 °C. It is observed that the dielectric constant and dielectric loss decrease with increasing frequency and attain saturation at higher frequencies. The low dielectric constant value of the crystal at high frequency is attributed to space charge polarization [25]. The very high value of dielectric constant at low frequencies is due to the presence of ionic, electronic and orientation polarizations.

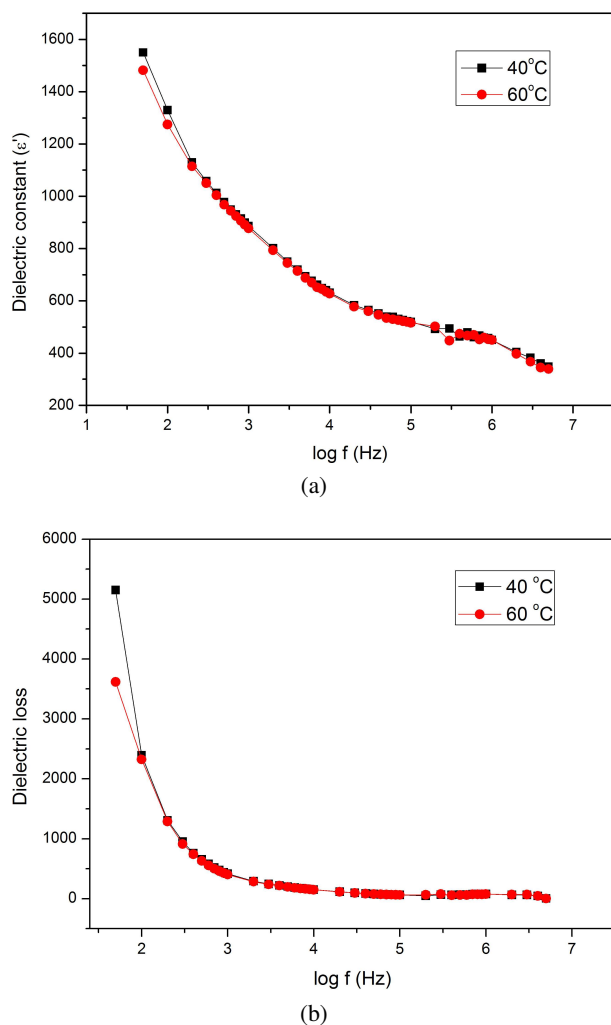


Fig. 8. Plots of dielectric constant (a) and dielectric loss (b) vs. $\log f$ for DSDMS.

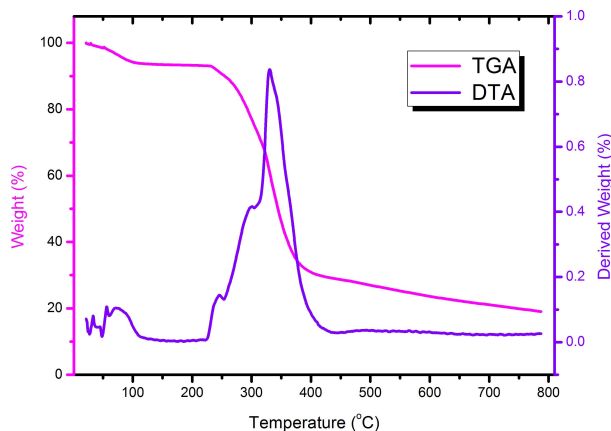


Fig. 9. Plot of thermogravimetric (TG-DTA) analysis for DSDMS.

Thermogravimetric (TG) and differential thermal analysis (DTA) are quite useful tools since they provide reliable information on the physico-chemical parameters. They characterize the process of transformation of solids or participation of solids in the process of isothermal or non-isothermal heating. Thermogravimetric analysis measures the change in mass of a sample on heating. TG-DTA plot of DSDMS is shown in Fig. 9. The endothermic peak in DTA observed at 330.7 °C illustrates the crystalline properties and melting point of DSDMS. Before melting there is decomposition at 58.52 °C due to the removal of moisture absorbed from the compound. The TGA curve clearly indicates that the DSDMS is stable upto 307.4 °C. After further heating the sample has undergone massive decomposition about 62 % which was due to release of pyridine moiety, SO_3 and other volatile gases. Finally, at the temperature of 750 °C, the residue mass was found about 19 %. It can be seen from the TG-DTA curve that the physical stability of DSDMS is appropriate to apply for device applications.

4. Conclusion

The organic nonlinear optical 4-N,N-dimethylamino-4'-N'-methylstilbazolium 2,4-dimethylbenzenesulfonate (DSDMS) single crystals were grown by slow evaporation. The positive solubility coefficient is convenient to grow DSDMS crystal by slow evaporation. The crystalline perfection, cell parameters and morphology have been identified for the grown crystal. From the morphology, the growth rate was found to be maximum along c-axis. Infrared and Raman spectral peaks confirmed the prominent bands corresponding to (C=C) and (C-C), SO_3 , CH_3 of the DSDMS. Optical cut-off wavelength of the DSDMS was found at 572 nm. Energy band gap was found to be 2.17 eV in the semi-conducting zone. Microhardness test confirmed the soft nature of the synthesised material while elastic stiffness constant (C_{11}) and yield strength (σ_v) were calculated for the grown crystal. The variation of dielectric constant and dielectric loss were studied as a function of frequency and temperature.

Thermal stability, decomposition stages and melting point of the DSDMS compound were studied. Hence, the present investigation reveals that the DSDMS crystal can be useful in the domain of nonlinear optical applications rather than its existing counterparts.

Acknowledgements

We thank Dr. P. K. Das, Department of Inorganic and Physical Chemistry, IISc, Bengaluru for providing SHG studies.

References

- [1] BOSSHARD C., SUTTER K., PRETRE P., HULLIGER J., FLORSHEIMER M., KAATZ P., GUNTER P., *Organic nonlinear optical materials*, Gordon and Breach, Amsterdam, 1995.
- [2] BOSSHARD C., BOSCH M., LIAKATAS I., JAGER M., GUNTER P., *Nonlinear Optical Effects and Materials*, Springer-Verlag, Berlin, 2000.
- [3] ZYSS J., *Molecular Nonlinear Optics: Materials, Physics and Devices*, Academic Press, New York, 1994.
- [4] HAMEED A.S.H., ANANDAN P., JAYAVEL R., RAMASAMY P., RAVI G., *J. Cryst. Growth*, 249 (2003), 316.
- [5] SHI Y., ZHANG C., ZHANG H., BECHTEL J.H., DALTON L.R., ROBINSON B., STEIER W., *Science*, 288 (2000), 119.
- [6] BENNER A.F., IGNATOWSKI M., KASH J.A., KUCHTA D.M., RITTER M.B., *J. Res. Dev.*, 49 (2005), 755.
- [7] LI L., CUI H., YANG Z., TAO X., LIN X., YE N., YANG H., *Cryst. Eng. Comm.*, 14 (2012), 1031.
- [8] SANKAR S., MANIKANDAN M.R., RAM S.D.G., MAHALINGAM T., RAVI G., *J. Cryst. Growth*, 312 (2010), 2729.
- [9] MARDER S.R., KIPPELEN B., JEN A.K., PEYGHAMBARIAN N., *Nature*, 388 (1997), 845.
- [10] SCHNEIDER A., NEIS M., STILLHART M., RUIZ B., KHAN R., GUNTER P., *J. Opt. Soc.*, 23 (2006), 1822.
- [11] KWON S., JAZBINSEK M., KWON O., GUNTER P., *Cryst. Growth Des.*, 10 (2010), 1552.
- [12] THAKUR M., TITUS J., MISHRA A., *Opt. Engg.*, 42 (2003), 456.
- [13] HOSOKAWA Y., ADACHI H., YOSHIMURA M., MORI Y., SASAKI T., MASUHARA H., *Cryst. Growth Des.*, 5 (2005), 861.
- [14] YANG Z., JAZBINSEK M., RUIZ B., ARAVAZHI S., GRAMLICH V., GUNTER P., *Chem. Mater.*, 19 (2007), 3512.
- [15] FIORAVANTI S., PELLACANI L., TARDELLA P.A., VERGARI M.C., *Org. Lett.*, 10 (2008), 1449.
- [16] EBITANI K., MOTOKURA K., MORI K., MIZUGAKI T., KANEDA K., *J. Org. Chem.*, 71 (2006), 5440.
- [17] RAJESH KUMAR P.C., RAVINDRACHARY V., JANARDHANA K., MANJUNATH H.R., KAREGOUDA P., CRASTA V., SRIDHAR M.A., *J. Mol. Struct.*, 1005 (2011), 1.
- [18] KASAP S., CAPPER P., *Springer Handbook of Electronic and Photonic Materials*, Springer Science Inc., 2006, pp. 47.
- [19] RAI R.N., MUDUNURI S.R., REDDI R.S.B., SATULURI V.S.A.K., GANESHMOORTHY S., GUPTA P.K., *J. Cryst. Growth*, 321 (2011), 72.
- [20] ONITSCH E.M., *Mikroskopie*, 2 (1947), 131.
- [21] HANNEMAN M., *Metall. Manchu*, 23 (1941), 135.
- [22] HAYS C., KENDALL E.G., *Metallography*, 6 (1973), 275.
- [23] WOOSTER W.A., *Rep. Prog. Phys.*, 16 (1953), 62.
- [24] MARY L.J., PRIYA M.N.S., DINAKARAN S., JEROME DAS S., *Cryst. Res. Technol.*, 43 (2008), 806.
- [25] RAO K.V., SMAKULA A., *J. Appl. Phys.*, 36 (1965), 2031.

Received 2016-04-06

Accepted 2016-09-28